Impact of Slot/Pole Combination on Inter-Turn Short-Circuit Current in Fault-Tolerant Permanent Magnet Machines

AQ:1 Jiri Dusek, Puvan Arumugam, Christopher Brunson, Emmanuel K. Amankwah, Tahar Hamiti, and Chris Gerada

Power Electronics Machines and Control Group, Faculty of Electrical Engineering,
The University of Nottingham, Nottingham NG7 2RD, U.K.
Power Electronics Machines and Control Group, Faculty of Electrical Engineering,
The University of Nottingham, Ningbo 315100, China

This paper investigates the influence of the slot/pole (S/P) combination on inter-turn short-circuit (SC) current in fault-tolerant permanent magnet (FT-PM) machines. A 2-D sub-domain field computational model with multi-objective genetic algorithm is used for the design and performance prediction of the considered FT-PM machines. The electromagnetic losses of machines, including iron, magnet, and winding losses are systematically computed using analytical tools. During the postprocessing stage, a 1-D analysis is employed for turn–turn fault analysis. The method calculates self- and mutual inductances of both the faulty and healthy turns under an SC fault condition with respect to the fault locations, and thus SC fault current, considering its location. Eight FT-PM machines with different S/P combinations are analyzed. Both the performance of the machine during normal operation and induced currents during a turn–turn SC fault are investigated. To evaluate the thermal impact of each S/P combination under an inter-turn fault condition, a thermal analysis is performed using finite element computation. It is shown that low-rotor-pole-number machines have a better fault tolerance capability, while high-rotor-pole-number machines are lighter and provide higher efficiency. Results show that the influence of the S/P selection on inter-turn fault SC current needs to be considered during the design process to balance the efficiency and power density against fault-tolerant criteria of the application at hand.

***Index Terms*—Fault tolerance (FT), inter-turn, permanent magnet (PM), short circuit (SC), slot/pole (S/P), synchronous machine.**

I. Introduction

PERMANENT magnet (PM) machines are attracting a large amount of attention in aerospace applications due to their high torque and consequently power density [1]–[5]. These machines are required to be safe, reliable, and available under tight weight, volume, and cost constraints. To meet all these demands, design tradeoffs are usually made to balance these design requirements [6].

The common design approach is adoption of fault-tolerance (FT) features within the electrical drive system. Such FT features allow the machine to fail safely, without any catastrophic damage and enable the machine to maintain the same or comparable performance under fault to that when the machine was healthy.

The most commonly implemented method of FT is redundancy [7]. However, adding redundancy increases the system weight, volume, and cost. In systems where $N + 1$ redundancy cannot be achieved due to these constraints, alternative FT features must be considered [8]. A number of FT features can be included in PM machine designs that increase the availability of the machine without adding redundancy and its associated weight, volume, and cost [8]–[10], such as the following:

1) use of the concentrated single layer windings, which allow the phase windings to be separated physically and magnetically, as shown in Fig. 1;

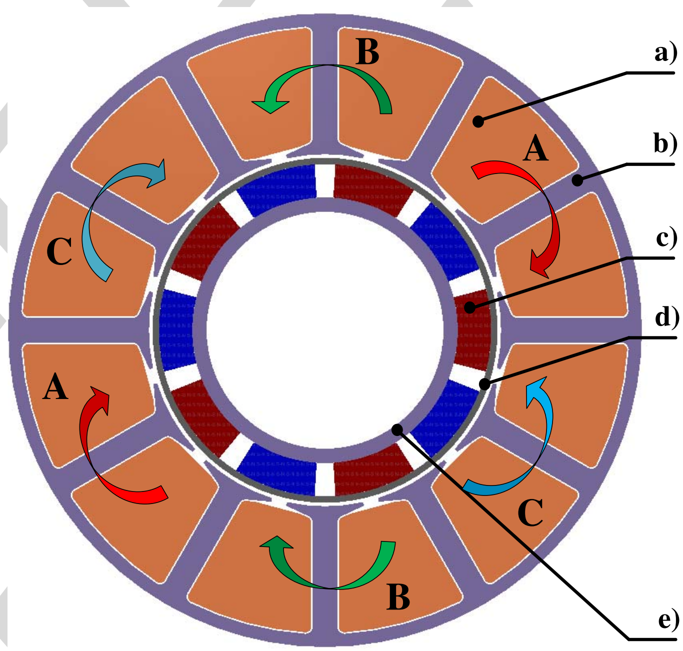

Fig. 1. Cross section of an FT-PM machine with single-layer concentrated winding. (a) Coil face of phase A. (b) Stator core iron. (c) PM. (d) Rotor sleeve. (e) Rotor core iron.

2) overrating of the phase inductance, which limits the phase short-circuit (SC) current to a safe value in the case of winding short-circuit fault;
3) designing the machine that is capable of withstanding increased current loading to deliver the rated output power during a fault, enabling continuous operation.

Manuscript received April 15, 2015; revised June 27, 2015 and September 1, 2015; accepted October 28, 2015. Corresponding author: J. Dusek (e-mail: jiri.dusek@nottingham.ac.uk).

Color versions of one or more of the figures in this paper are available online at http://ieeexplore.ieee.org.

Digital Object Identifier 10.1109/TMAG.2015.2500894

0018-9464 © 2015 IEEE. Personal use is permitted, but republication/redistribution requires IEEE permission.
See http://www.ieee.org/publications_standards/publications/rights/index.html for more information.

Although the above-mentioned features improve the FT of the machine, they also reduce the torque density of the machine. However, a design using these features has an advantage over a system using redundancy in terms of weight, volume, and cost, as the system is not duplicated.

The key fault in such FT design is the inter-turn SC fault, which cannot be completely mitigated due to the permanent magnetic field. During inter-turn SC fault, post-fault control methods are often adopted to minimize the fault current [11]–[13]. The most common post-fault control method involves shorting the machine terminals [13]. This method is easy to implement via a converter without the need for any additional hardware. However, this method requires large winding inductances so that the SC current is limited to a safe value. In general, designs with 1 pu phase inductance are preferred solutions to limit the SC current [8].

Although this is effective for many turn–turn faults, a single turn–turn (an inter-turn) fault is still problematic, because the fault current mainly depends on the turn inductance, which depends on the location of the fault in the slot. More importantly, an inter-turn fault occurring close to the slot-opening region experiences a high SC current due to its low inductance [9], [14].

This paper investigates the influence of the slot/pole (S/P) combination on the inter-turn SC fault in an FT-PM machine. The study considers applications where it is safe to short the terminals of the machine windings as part of the post-fault control. Using analytical tools, a set of machines with different S/P combinations are studied. A 2-D sub-domain field computational model with multi-objective GA is used for design and performance prediction of the studied machines, where the electromagnetic losses including iron, magnet, and winding losses are systematically calculated. 1-D analysis is employed for turn–turn fault prediction by calculating the self- and mutual inductances of both the faulty and healthy turns during an SC fault condition with respect to the fault locations and thus fault current. The obtained results show that the SC fault current is highly influenced not only by the position in the slot where the inter-turn fault occurs, but also by the selected slot and pole number. It has been shown that the inter-turn fault current becomes significant with high pole numbers machines.

II. Background

Because FT-PM machines have alternate tooth wound concentrated windings that provide magnetic isolation between phases, mutual coupling is negligibly small [15]. Thus, the electrical circuit representing the phase winding during a turn–turn SC fault can be described using the differential equations (1) and (2), which represent the healthy turns and the faulty turns, respectively

$$V_1(t) = I_1(t)R_h + L_h\frac{dI_1}{dt} + L_m\frac{dI_s}{dt} + e_1(t) \quad (1)$$

$$0 = I_s(t)R_s + L_s\frac{dI_s}{dt} + L_m\frac{dI_1}{dt} + e_2(t) \quad (2)$$

where

- e_1 electro motive force in the healthy turns;
- e_2 electro motive force in the shorted turns;
- I_1 phase current induced in the shorted turns;
- I_s SC fault current;
- L_h self-inductance of the healthy turns;
- L_s self-inductance of the shorted turns;
- L_m mutual inductance between the healthy and the shorted turns;
- R_h resistance of the healthy turns;
- R_s resistance of the shorted turns.

Hence, the steady-state SC fault current (I_s), after the machine has been shorted via the converter terminals, can be estimated using the following equation:

$$I_s = \frac{j\omega_e L_m}{R_s R_h + \omega_e{}^2({L_m}^2 - L_s L_h) + j\omega_e(R_h L_s + R_s L_h)}e_1 - \frac{j\omega_e L_h + R_h}{R_s R_h + \omega_e{}^2({L_m}^2 - L_s L_h) + j\omega_e(R_h L_s + R_s L_h)}e_2 \quad (3)$$

where ω_e is the angular electrical pulsation. From (3), it can be seen that I_s is related to three major parameters, which are resistances R_s and R_h, inductances L_h, L_s and L_m, and operational frequencies.

For clarity, the terms in (3) can be substituted as follows:

$$\begin{cases} a = {L_m}^2 - L_s L_h \\ b = R_h L_s + R_s L_h \\ c = R_s R_h. \end{cases} \quad (4)$$

With electromotive forces expressed as

$$\begin{cases} e_1 = \omega_e \varphi N_h \\ e_2 = \omega_e \varphi N_s \end{cases} \quad (5)$$

where N_h and N_s are the number of healthy and shorted turns, respectively. Substituting (4) and (5) into (3) yields

$$I_s = \frac{jL_m\omega_e}{a\omega_e{}^2 + b\omega_e + c}\omega_e\varphi N_h - \frac{jL_h\omega_e + R_h}{a\omega_e{}^2 + b\omega_e + c}\omega_e\varphi N_s \quad (6)$$

where φ represents the non-load flux linkage per turn. Dividing the nominator and denominator of (6) by $\omega_e{}^2$ yields AQ:2

$$I_s = \frac{jL_m\varphi N_h - jL_h\varphi N_s - \varphi N_s\frac{R_h}{\omega_e}}{a + j\frac{b}{\omega_e} + \frac{c}{\omega_e{}^2}}. \quad (7)$$

As ω_e is significantly greater than b, c, and R_h, (7) can be simplified to

$$I_s = \frac{jL_m\varphi N_h}{a} - \frac{jL_h\varphi N_s}{a}. \quad (8)$$

For the considered single turn-turn fault condition, $N_s = 1$; therefore, the second term of (8) can be neglected

$$I_s = \frac{jL_m\varphi N_h}{a}. \quad (9)$$

IEEE Proof

TABLE I
DESIGN REQUIREMENTS OF THE FT-PM MACHINE

Parameter	Value
Stator outer diameter (OD)	120mm
Rated speed	2000rpm
DC link voltage	270V
Phase self-inductance	1pu
Rated torque	10Nm
Split ratio (SR)	Variable
Tooth-width ratio (TR)	Variable
Axial length (l_{stk})	Variable
Aspect ratio (AR)	l_{stk}/OD
Slot opening (So)	Variable
Tooth height (h_t)	Variable
Magnet height (h_m)	Variable
Number of turns per slot (N_t)	Variable
Phase current (I_p)	Variable

Substituting the original term for a from (4) into (9) yields

$$I_s = \frac{jL_m\varphi N_h}{{L_m}^2 - L_sL_h} = \frac{j\varphi N_h}{L_m - \frac{L_sL_h}{L_m}}. \tag{10}$$

As the second term of the denominator (L_sL_h/L_m) in (10) is significantly smaller than the first term of the denominator L_m, it can be neglected and the equation can be expressed as

$$I_s = \frac{j\varphi N_h}{L_m}. \tag{11}$$

From (11), it is evident that the steady-state SC fault current I_s is proportional to the number of turns and inversely proportional to the mutual inductances between healthy and faulty turns. As with increasing pole number both the number of turns per slot and mutual inductance between the healthy and faulty turns reduce, it is not evident how the S/P combination influences the SC fault current. Therefore, a detailed analysis has to be performed to draw such a conclusion.

III. SELECTION OF THE SLOT/POLE COMBINATION

As mentioned earlier, alternate tooth wound concentrated winding topologies are often preferred in FT applications due to the physical and magnetic isolation between the phases [16], [17]. Due to the inherent FT capability, a number of FT-PM machines with different S/P combinations are selected for the ensuing studies. In total, eight S/P combinations have been considered for this study, specifically, 6/4, 12/8, 12/10, 12/14, 18/12, 24/16, 24/20, and 24/28. The design specifications, together with the considered design variables, are presented in Table I. The aim of the selection of S/P combinations is to compare a reasonable number of S/P cases to obtain a set of data that will provide insight into the influence of S/P combination on SC fault current. The slot number is selected as a multiple of six (12, 18, 24) in a way to accommodate three phase windings and alternate tooth winding arrangements. For the slot number selected, a number of pole combinations could be considered. In this paper, a number of poles for each slot configuration have been considered to investigate the characteristics of the particular machine designs during fault. The selected S/P combinations, though not exhaustive, are considered significant enough to demonstrate such influence.

IV. FT-PM MACHINE MODELING

Fig. 2 represents the process involved in the optimization of the electrical machine design and both the performance and turn–turn SC fault analysis of the optimized design. The optimization process starts with the initially selected S/P combinations in Section III and the fixed outer diameter (OD) of 120 mm, which is limited by the envelope of the target application. Other design variables such as split ratio (SR), aspect ratio (AR), tooth-width-to-slot ratio (TR), slot-opening (So), tooth-tip height (h_t), magnet span (α_m), magnet height (h_m), the number of turns per slot (N_t), and phase current (I_p) are set as variable parameters. The design process is limited by the following three design constraints.

1) A maximum no-load air-gap flux density of 0.9 T.
2) Phase winding inductances are overrated to have 1 pu inductance in order to limit the phase SC current equivalent to rated phase current of the design.
3) DC link voltage limit of the converter is fixed to ±135 V.

The key design optimization target is to produce highly efficient and high-mass-density PM machines while satisfying the above-mentioned constraints and application requirements given in Table I. A multi-objective GA is adopted for the optimization process, in which a 2-D electromagnetic model is used during the design process, while to investigate the turn–turn SC fault current, the 1-D SC fault model is used. It is worth noting that by adopting an analytical model for the design and analysis, the computation time is greatly reduced while maintaining a high level of accuracy. Finite element (FE) is therefore not considered here. The adopted analytical model and the GA technique for the design and analysis are discussed in detail in the following sections.

A. 2-D Sub-Domain Field Model

The analytical model is based on a sub-domain field model that solves Maxwell's equations in polar coordinates considering the associated boundary conditions of each domain. In order to establish the model, the machine geometry is divided into four sub-domains: 1) rotor PM sub-domain (A_{I}, region I); 2) air-gap sub-domain (A_{II}, region II); 3) slot-opening sub-domain (A_i, region III, $i = 1, 2 \ldots Q$); and 4) stator slot sub-domain (A_j, region IV, $j = 1, 2 \ldots Q$), as shown in Fig. 3. The following assumptions were made.

1) The machine has a radial geometry as shown in Fig. 3.
2) The stator and rotor cores have an infinite permeability and zero conductivity.
3) The magnets are magnetized in the radial direction and their relative recoil permeability is unity ($\mu_r = 1$).
4) The current density (J_c) over the slot area is uniformly distributed.
5) The end-effects are neglected and thus the magnetic vector potential has only one component along

IEEE Proof

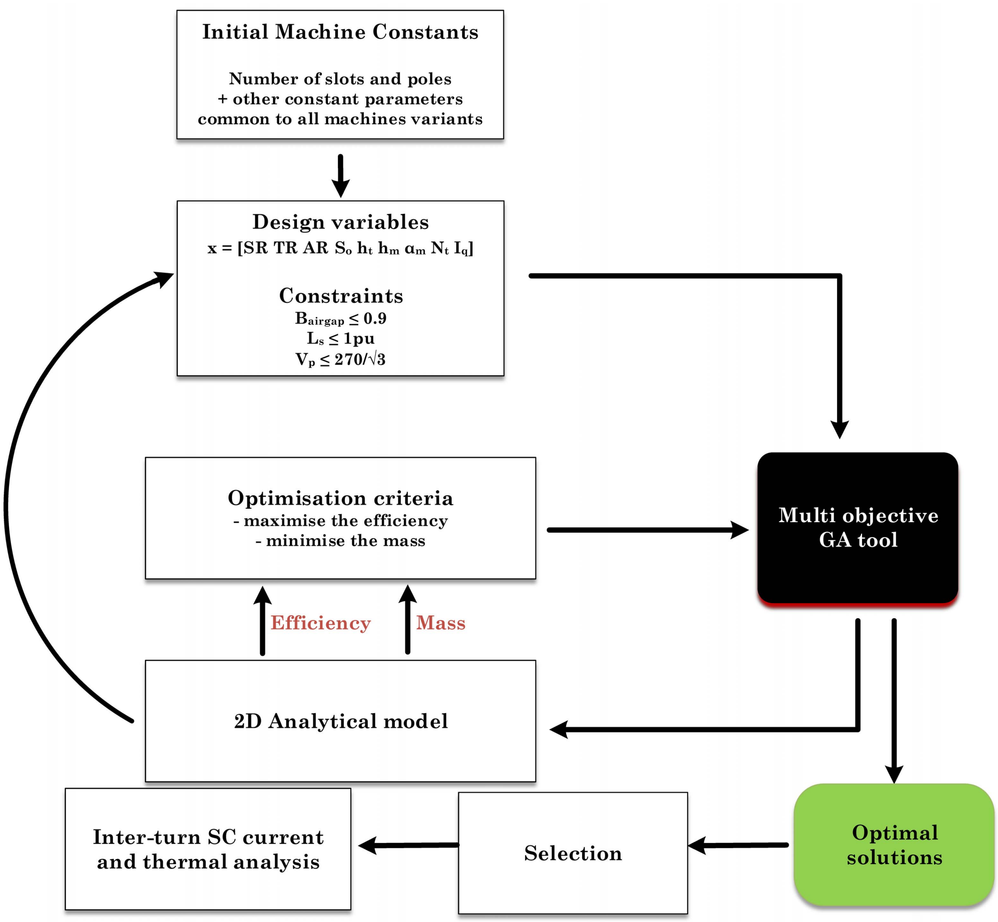

AQ:3

Fig. 2. Flowchart of the machine optimization process and performance analysis.

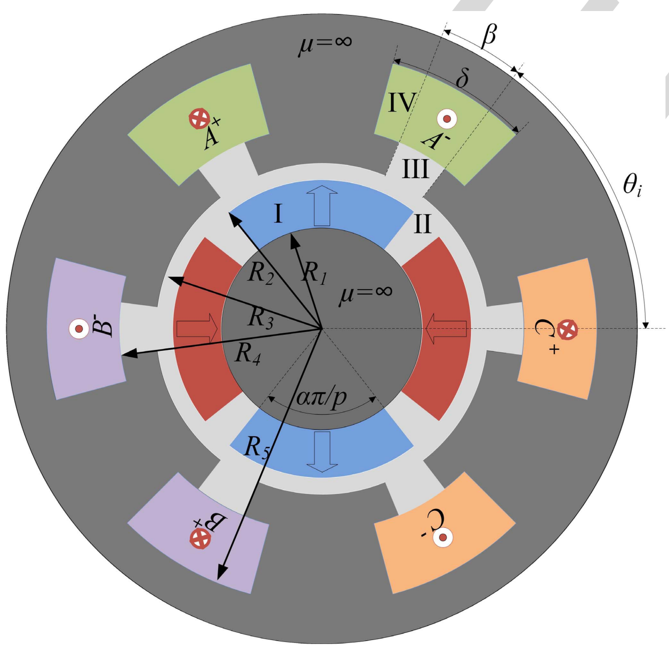

Fig. 3. Axial cross section of a 6-slot, 4-pole FT-PM machine.

the z direction and it only depends on the polar coordinates r and θ.

6) The walls of the slot are finely laminated so that the effect of eddy currents within the iron can be neglected.

The magnetostatic partial differential equations governing in the behavior of the machine in the different sub-domains can be derived from Maxwell's equations.

These equations are formulated in terms of vector potential as in

$$\begin{cases} \frac{\partial^2 A_{\mathrm{I}}}{\partial r^2} + \frac{1}{r}\frac{\partial A_{\mathrm{I}}}{\partial r} + \frac{1}{r^2}\frac{\partial^2 A_{\mathrm{I}}}{\partial \theta^2} = \frac{-\mu_o}{r}\frac{\partial M_r}{\partial \theta} \\ \frac{\partial^2 A_{\mathrm{II}}}{\partial r^2} + \frac{1}{r}\frac{\partial A_{\mathrm{II}}}{\partial r} + \frac{1}{r^2}\frac{\partial^2 A_{\mathrm{II}}}{\partial \theta^2} = 0 \\ \frac{\partial^2 A_i}{\partial r^2} + \frac{1}{r}\frac{\partial A_i}{\partial r} + \frac{1}{r^2}\frac{\partial^2 A_i}{\partial \theta^2} = 0 \\ \frac{\partial^2 A_j}{\partial r^2} + \frac{1}{r}\frac{\partial A_j}{\partial r} + \frac{1}{r^2}\frac{\partial^2 A_j}{\partial \theta^2} = -\mu_o J_c \end{cases} \quad (12)$$

where A represents the magnetic vector potential and its subscript is related to the associated sub-domains. μ_0 is the permeability of air, J_c is the current density, and M_r is the magnetization radial component. Employing the separation of variables method in each sub-domain, the general solution can be obtained [18], [19]. A detailed solution of (12) can be found in [18]. Since the magnetic vector potential is known everywhere in each domain, the performance of the machine can be calculated [18], [19].

B. Performance Estimation

Using the Maxwell stress tensor, the electromagnetic torque can be calculated by considering a circle of radius r_c in the air-gap sub-domain as the integration path. Hence, the electromagnetic torque can be given as follows:

$$T_e = \frac{l_{\text{stk}} r_c}{\mu_o} \int_0^{2\pi} {B_r}^{\text{II}}(r_c,\theta) {B_\theta}^{\text{II}}(r_c,\theta) d\theta \tag{13}$$

where

$${B_r}^{\text{II}} = \frac{1}{r}\frac{\partial A_{\text{II}}(r,\theta)}{\partial \theta} \tag{14}$$

$${B_\theta}^{\text{II}} = -\frac{\partial A_{\text{II}}(r,\theta)}{\partial r} \tag{15}$$

and l_{stk} is the axial length of the machine, μ_0 is permeability of air, and B_r and B_θ are radial and tangential component in the air gap sub-domain, respectively.

In order to estimate both the self-inductance (L_p) and the voltage (V_p) of the phase windings, the flux linkage associated with the cross section of each slot (A_s) with respect to the rotor position (θ), need to be determined. The flux linkage associated with each coil can be represented by averaging the vector potential over the slot area considering the assumption (15) in the model. Thus, the flux can be described by

$$\phi = \frac{l_{\text{stk}}}{A_s} \int\int_{A_s} A_j(r,\theta) r dr d\theta. \tag{16}$$

Hence, the phase self-inductance and voltage can be represented as a function of flux as described in

$$L_p = \frac{\phi N_{\text{ph}}}{J_c A_s K_f} \tag{17}$$

$$V_p = -N_{\text{ph}} \omega \frac{\partial \phi}{\partial \Theta} \tag{18}$$

where N_{ph} is the number of turns per phase, K_f is the fill factor, and ω is the rotor angular speed.

For the efficiency evaluation, the losses associated with the machine are calculated. The three main loss components, winding losses, iron losses, and eddy current losses in the magnet, are considered, while the mechanical losses are neglected. The winding losses consist of both eddy current losses in the slot and dc losses, which take into account both the losses in the slot and the end windings.

To estimate the winding eddy current losses in the slot, the magnetic vector potential obtained in the slot is used. The eddy current density (J_e) and the associated copper losses (P_c) in a conductor are estimated using (19) and (20), respectively

$$J_e = -\sigma \frac{\partial A_j}{\partial t} + C(t) \tag{19}$$

$$P = \frac{\omega l_{\text{stk}}}{2\pi\sigma} \int_0^{2\pi/\omega_{rm}} \int_{r_{c1}}^{r_{c2}} \int_{\theta_{c1}}^{\theta_{c2}} J_e^2 r \, dt \, d\theta \, dr \tag{20}$$

where A_j is magnetic vector potential in the jth slot, σ is the conductivity, and r_{c1}, r_{c2}, σ_{c1}, and σ_{c2} are the radial and tangential coordinates delimiting the cross-sectional area of interest. In a similar manner, the eddy current losses associated with the magnet are estimated using the magnetic vector potential obtained in the magnet sub-domain.

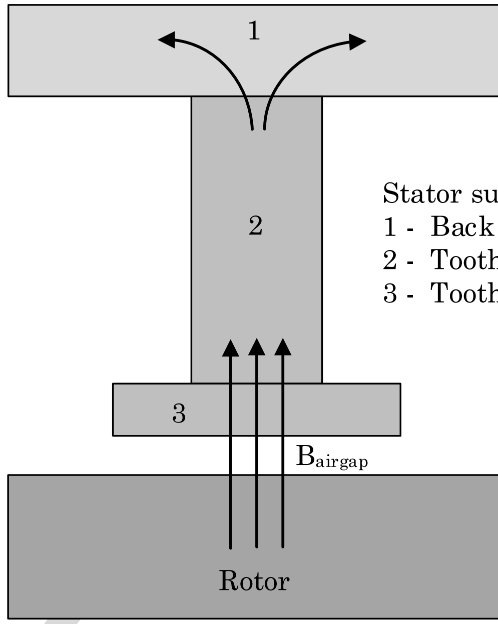

Fig. 4. Illustration of the stator partition for the purpose of the stator iron losses estimation.

Both hysteresis and eddy current losses associated with the stator iron are estimated using the well-known Steinmetz equations, where the losses generated due to localized saturation phenomena are neglected. As given in Fig. 4, the stator iron is divided into three parts. The flux density in each part is evaluated considering the average flux density in the air-gap domain. Finally, the iron losses are estimated using the evaluated flux density together with the material properties from its associated data sheet. It is worth highlighting here that the flux density harmonic effects in localized point and time harmonics associated with pulsewidth modulation (PWM) are not accounted for.

Since the total electromagnetic losses (P_t) are known, the efficiency (η) can be obtained from

$$\eta = \frac{T_e \omega}{P_t + T_e \omega}. \tag{21}$$

C. Optimization Process of the Design

The design process is carried out using an optimization routine based on a non-dominated sorting genetic algorithm, where the above-mentioned 2-D electromagnetic computational methodology is integrated to evaluate the performance [20]. The goal of the GA is to maximize the efficiency and minimize the mass of the machine. As previously mentioned, the optimization envelope was constrained by the no-load air-gap flux density (B_{airgap}), phase self-inductance (L_p), and converter voltage limit. The per-unit base inductance L_{pu} is set as follows:

$$L_{\text{pu}} = \frac{\Psi_{\text{PM}}}{I_p} \tag{22}$$

where Ψ_{PM} is flux linkage due to the permanent magnets and I_p is the rated phase current of the machine. Thus, the SC fault current during a fault will be limited to its nominal value.

IEEE Proof

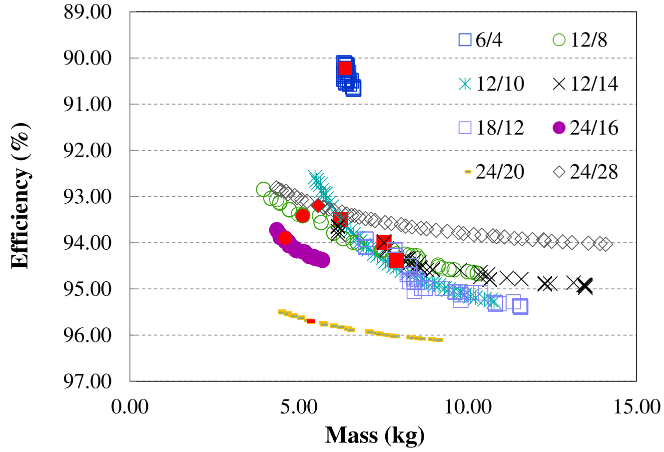

Fig. 5. Pareto-optimal sets for analyzed machines.

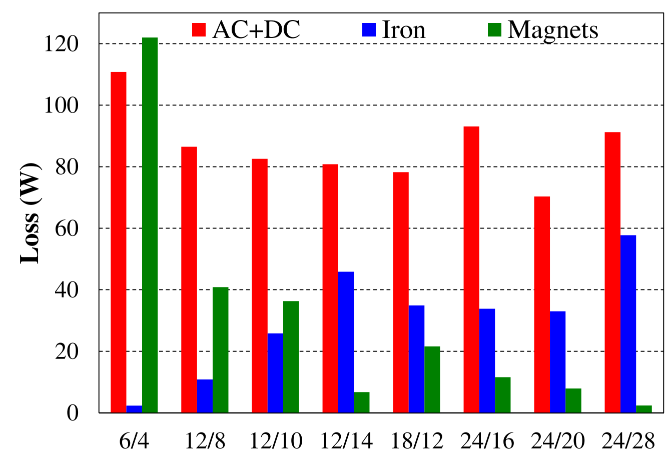

Fig. 6. Comparison of the individual losses across the studied machines (ac + dc represents ac and dc copper losses, including the end winding losses; Iron and Magnets represents eddy current and hysteresis losses in the stator iron and magnets, respectively).

TABLE II
OPTIMIZED DESIGN PARAMETERS OF THE MACHINES

S/P	SR	TR	AR	H_m	N_t	Stator Mass	Machine Weight	η
[-]	[-]	[-]	[-]	[mm]	[-]	[kg]	[kg]	[%]
6/4	0.65	0.64	0.67	3.1	92	2.20	6.41	90.15
12/8	0.65	0.64	0.56	4.4	52	1.98	5.12	93.41
12/10	0.67	0.46	0.68	4.3	38	2.61	6.28	93.55
12/14	0.69	0.43	0.82	3.9	32	3.06	7.52	94.05
18/12	0.59	0.59	0.89	4.6	26	3.31	7.85	94.37
24/16	0.68	0.52	0.60	4.4	24	2.13	4.60	93.89
24/20	0.69	0.55	0.70	4.5	23	2.30	5.26	95.70
24/28	0.69	0.51	0.74	4.7	20	2.50	5.57	93.17

The machine is chosen for analysis once the GA generates a set of Pareto-optimal solutions of the multi-objective optimization problem that satisfies both the optimization criteria and constrains. The obtained Pareto-optimal sets for all analyzed machines are shown in Fig. 5. As in an aerospace application oriented study, lower mass is prioritized over the efficiency and therefore the set of the parameters is selected at the end of first quarter of the Pareto front with the respect to the mass. The red points in Fig. 5 highlighting the machines selected for the SC fault analysis are presented in the paper. The design parameters of the selected machines for different S/P combinations are summarized in Table II.

D. SC Current Calculation

Once the machine design has been finalized, the SC analysis is carried out at the post processing stage. A simplified 1-D analytical method proposed in [9] is adopted for this study. The 1-D model used to predict the SC current is computed during postprocessing. A 2-D model can be considered, but it involves solving the problem in each conductor sub-domain instead of in the slot sub-domain. This would significantly increase the evaluation time of the considered optimization process. The adopted model estimates the inductances during an SC fault condition, considering that the short-circuited turn is surrounded by the remaining healthy turns. This facilitates the accurate prediction of the leakage fluxes; consequently, the inductances can be determined, and considering the total winding resistance, the fault current can be calculated [9].

V. RESULTS AND DISCUSSION

In this section, results from the investigation of the effect of S/P combination on inter-turn SC current in FT-PM are presented. This section is divided into three subsections, where the outcomes of the individual analyses are explained. Losses and SC fault current were analyzed for each S/P combination and thermal analysis was performed for the selected S/P variants. In addition, a method that minimizes the SC fault current is proposed.

A. Losses and Efficiency of the Studied Machines

The loss breakdown for each of the machines studied is shown in Fig. 6. While the ac and the dc winding losses are a major part of the total losses in all cases, the low slot number machines show high winding losses. The increase in the winding losses is mainly due to the bigger end windings' length of the machines with a low slot number. The high-pole-number machines have high iron losses due to the higher electrical frequency necessary for their operation. Also it is worth noting that the 12/14 machine has higher iron losses than the 24/16 and 24/20 machines. The stator iron loses are dictated not only by the fundamental frequency of the phase current, but also by the mass of the machine's stator core. As is shown in Table II, the mass of the 12/14 machine's stator core is bigger than the mass of both 24/16 and 24/20 machines' stator core and so are the iron losses of the 12/14 machine.

From Figs. 6 and 7, it can be seen that the 6/4 machine proved to have the highest losses and thus lowest efficiency. This is mainly due to high winding losses and magnet eddy current losses. If the segmentation is adopted for the machine, the magnet eddy current losses can be reduced. Although this would be possible, the resultant efficiency will depend on the number of segments adopted in the design.

As can be seen from Fig. 7, it is obvious that among the considered machines, the 24/20 machine variant, which delivers rated output with 95.7% efficiency, is the best design choice in terms of performance.

IEEE Proof

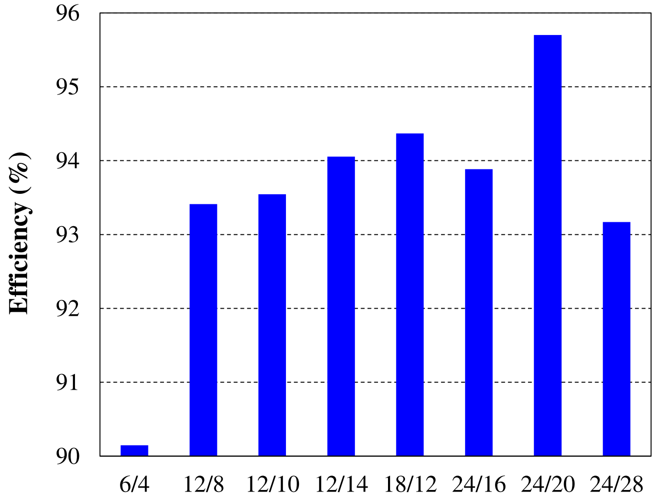

Fig. 7. Comparison of efficiencies across the studied machines.

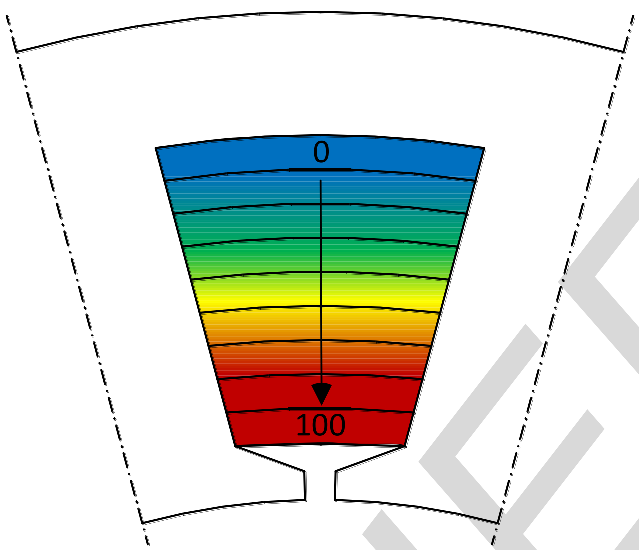

Fig. 8. Illustration of an inter-turn SC fault location reference in a slot.

B. Short-Circuit Current in the Faulty Turn

As explained earlier, the results of the SC analysis are based on a 1-D analytical approach. In the analysis, the position of the faulty turn in the slot is expressed by the relative position, where 0 corresponds to the outer border of the slot and 100 corresponds to the inner border of the slot, which is close to the slot-opening, as shown in Fig. 8. The obtained SC fault currents with respect to the location are given in Fig. 9.

Clearly, for all the analyzed machines, the highest SC current is observed when the inter-turn fault occurs near the slot-opening area. It is worth noting that the magnitude of the SC fault current increases with increasing pole number.

Although the S/P combination of 24/20 variant has higher efficiency, it produces the largest SC fault current of more than 5 pu. If the focus is mainly given to the FT, the 6/4 variant is the best candidate among the machines analyzed. This clearly explains that a balanced tradeoff between efficiency and FT is required for the design of machines for applications where FT is desired.

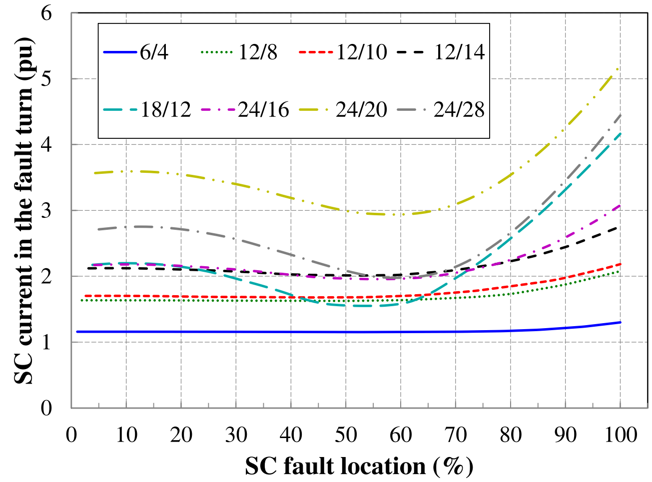

Fig. 9. Inter-turn SC fault current versus fault location in a slot (0 and 100 represent locations close to the inner and outer boundary of the slot, respectively).

Among other candidates, S/P combinations of the 12/8 and 12/10 machines have a similar SC behavior. It can also be seen in S/P combinations of the 12/14 machine and 24/16 machine. This is because of the associated electrical frequencies, which are almost equal. Although these pairs of machines provide almost identical results regarding SC, in terms of efficiency, the 12/8 and 12/14 machines show increased efficiency.

C. Thermal Analysis of the Studied Machines

In order to visualize the thermal behavior, the thermal analysis was performed using the FE software and was carried out in a coupled electromagnetic and thermal FE environment. Two states, healthy and faulty, are studied. The healthy state is simulated with a nominal phase current.

For the faulty state, to minimize the evaluation time, the steady-state SC current obtained in the inter-turn SC fault analysis is injected into the faulty turn. The remaining healthy windings are separately excited using the nominal phase current. In the analysis, thermal continuity between stator and rotor is taken into account and the thermal boundaries (stator outer surface temperature is fixed to 120 °C) are kept the same for all cases. The conductors' cross-sectional area and insulation thickness are carefully selected considering slot fill factor $K_f = 0.5$. Results obtained for four cases are presented in Fig. 10.

The SC analysis proved that the 6/4 machine is the most tolerant to the inter-turn SC fault, and the difference in the thermal distribution in the slot between the healthy and fault conditions is almost negligible. As expected, high-pole-number variants 24/16 and 24/20 show a noticeable temperature rise at the fault condition. Fig. 10(g) and (h) shows that the 24/20 machine variant has critical hotspot due to the larger fault current. It is worth highlighting here that although the 24/16 machine variant is subjected to less magnitude of worst case SC current than the 18/12 variant, it has poor thermal behavior. This is due to the windings resistance associated with the 24/16 machine variant, which is higher than in the 18/12 variant, as evident from Fig. 6.

IEEE Proof

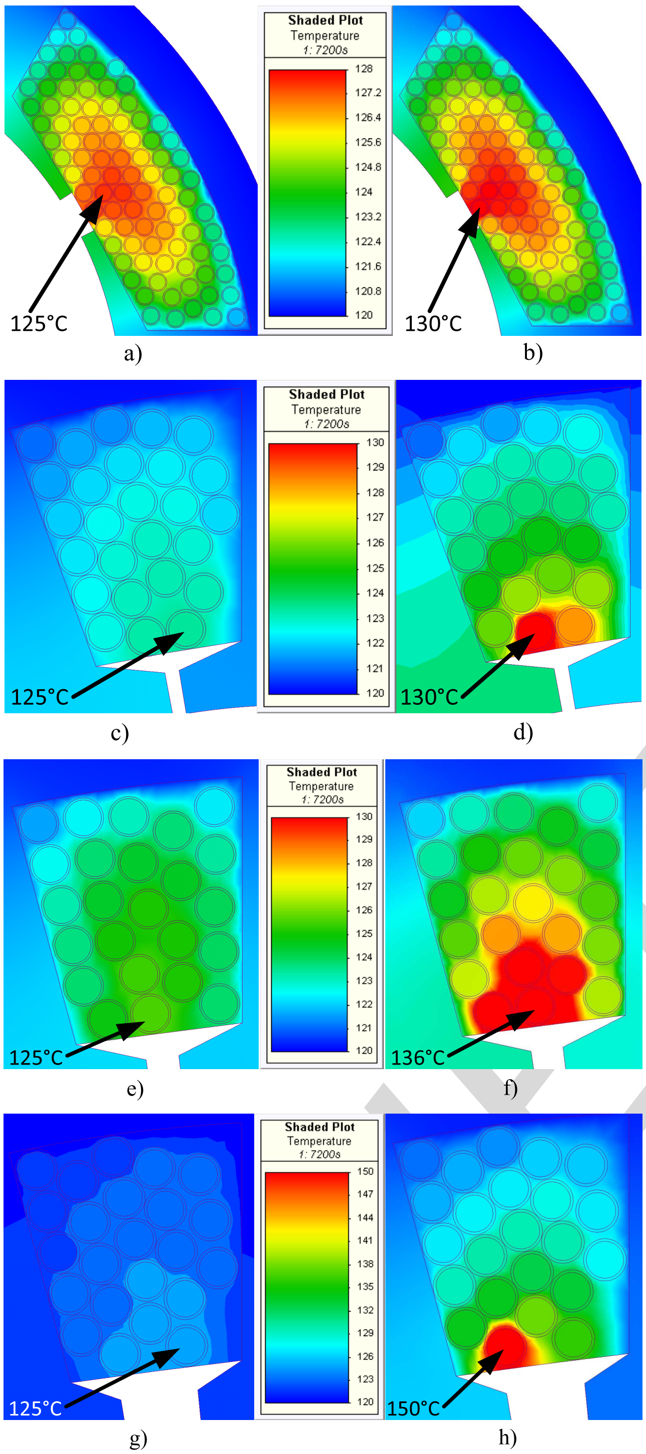

Fig. 10. Thermal distribution in a slot of 6-slot, 4-pole machine under (a) healthy and (b) faulty conditions; 18-slot, 12-pole machine under (c) healthy and (d) faulty conditions; 24-slot, 16-pole machine under (e) healthy and (f) faulty conditions; and 24-slot, 20-pole machine under (g) healthy and (h) faulty conditions.

From the analysis and the results presented in Figs. 9 and 10, it can be summarized that the analyzed low-pole-number PM machines are suitable for FT design although they have low efficiency compared with the analyzed high-pole-number machines. Overall, the 12/8 and 12/10 machine variants proved to be the best compromise for such FT designs, since they have higher efficiency and the SC current is almost twice the rated value.

D. Modifications Toward SC Current Reduction

Although the 12/8 and 12/10 machine variants are the best choice in terms of FT and efficiency, those machines have almost twice the rated current when fault occurs close to the slot-opening region. One way of minimizing the fault current is to design the machine with a larger inductance, which can be even higher than one per unit inductance. When possible, this would result in a lower power factor and a significant reduction in the achievable torque density.

Alternatively, the maximal SC current can be maintained at twice the rated current by avoiding the placement of the winding closer to slot-opening region. From Fig. 9, it is obvious that using only 90% of the slot for the winding and avoiding 10% closest to the slot-opening region replaces the maximal SC fault current significantly. For the 12/8 and 12/10 machine variants, the SC current can be limited to under 2 pu, if the 10% slot region is avoided. However, this will reduce the slot fill factor, consequently increasing the dc losses. However, it would be beneficial if the machine is operated at high speeds, as the ac losses would be reduced [21].

VI. CONCLUSION

In this paper, the influence of the S/P combination on inter-turn SC fault in FT-PM machines has been investigated. Parameters of eight machines with different S/P combinations have been optimized using GA optimization and 2-D analytical model. Efficiency and inter-turn SC fault behaviors have been analyzed for each of the machines.

It has been shown that the most critical inter-turn fault location is near the slot-opening region and the magnitude of the SC fault current can be significantly reduced by avoiding winding placement near this region.

Furthermore, the inter-turn fault current magnitude depends on the selection of the slot and pole numbers, which influence the windings' parameters, namely, resistance and self-inductance of both healthy and faulty turns and mutual inductance between them.

Lower S/P combinations have better FT capability, while high S/P combinations have improved efficiency. To balance the efficiency and FT criteria of the application, the impact of the S/P combination on inter-turn SC fault current must be considered for the design process.

REFERENCES

[1] P. E. Kakosimos, E. M. Tsampouris, and A. G. Kladas, "Design considerations in actuators for aerospace applications," *IEEE Trans. Magn.*, vol. 49, no. 5, pp. 2249–2252, May 2013.

[2] J.-C. Urresty, J.-R. Riba, and L. Romeral, "A back-EMF based method to detect magnet failures in PMSMs," *IEEE Trans. Magn.*, vol. 49, no. 1, pp. 591–598, Jan. 2013.

[3] J. Li, K. T. Chau, J. Z. Jiang, C. Liu, and W. Li, "A new efficient permanent-magnet vernier machine for wind power generation," *IEEE Trans. Magn.*, vol. 46, no. 6, pp. 1475–1478, Jun. 2010.

[4] J.-R. Riba Ruiz, J. A. Rosero, A. G. Espinosa, and L. Romeral, "Detection of demagnetization faults in permanent-magnet synchronous motors under nonstationary conditions," *IEEE Trans. Magn.*, vol. 45, no. 7, pp. 2961–2969, Jul. 2009.

[5] J. Wang, K. Atallah, and D. Howe, "Optimal torque control of fault-tolerant permanent magnet brushless machines," *IEEE Trans. Magn.*, vol. 39, no. 5, pp. 2962–2964, Sep. 2003.

[6] W. Cao, B. C. Mecrow, G. J. Atkinson, J. W. Bennett, and D. J. Atkinson, "Overview of electric motor technologies used for more electric aircraft (MEA)," *IEEE Trans. Ind. Electron.*, vol. 59, no. 9, pp. 3523–3531, Sep. 2012.

[7] C. Gerada and K. J. Bradley, "Integrated PM machine design for an aircraft EMA," *IEEE Trans. Ind. Electron.*, vol. 55, no. 9, pp. 3300–3306, Sep. 2008.

[8] P. Arumugam, T. Hamiti, C. Brunson, and C. Gerada, "Analysis of vertical strip wound fault-tolerant permanent magnet synchronous machines," *IEEE Trans. Ind. Electron.*, vol. 61, no. 3, pp. 1158–1168, Mar. 2014.

[9] P. Arumugam, T. Hamiti, and C. Gerada, "Modeling of different winding configurations for fault-tolerant permanent magnet machines to restrain interturn short-circuit current," *IEEE Trans. Energy Convers.*, vol. 27, no. 2, pp. 351–361, Jun. 2012.

[10] B. C. Mecrow, A. G. Jack, J. A. Haylock, and J. Coles, "Fault-tolerant permanent magnet machine drives," *IEE Proc.-Electr. Power Appl.*, vol. 143, no. 6, pp. 437–442, Nov. 1996.

[11] K. Dooley and M. Dowhan. (2008). *Method and Apparatus for Controlling an Electric Machine*. [Online]. Available: http://www.google.com/patents/US7443070

[12] A. J. Mitcham, G. Antonopoulos, and J. J. A. Cullen, "Implications of shorted turn faults in bar wound PM machines," *IEE Proc.-Electr. Power Appl.*, vol. 151, no. 6, pp. 651–657, Nov. 2004.

[13] J. A. Haylock, B. C. Mecrow, A. G. Jack, and D. J. Atkinson, "Operation of fault tolerant machines with winding failures," *IEEE Trans. Energy Convers.*, vol. 14, no. 4, pp. 1490–1495, Dec. 1999.

[14] J. Dusek, P. Arumugam, T. Hamiti, and C. Gerada, "Selection of slot-pole combination of permanent magnet machines for aircraft actuation," in *Proc. Int. Conf. Elect. Syst. Aircraft, Railway, Ship Propuls. Road Vehicles*, Mar. 2015, pp. 1–5.

[15] A. M. El-Refaie, "Fault-tolerant permanent magnet machines: A review," *IET Electr. Power Appl.*, vol. 5, no. 1, pp. 59–74, Jan. 2011.

[16] G. Liu, J. Yang, W. Zhao, J. Ji, Q. Chen, and W. Gong, "Design and analysis of a new fault-tolerant permanent-magnet vernier machine for electric vehicles," *IEEE Trans. Magn.*, vol. 48, no. 11, pp. 4176–4179, Nov. 2012.

[17] A. S. Abdel-Khalik, S. Ahmed, A. M. Massoud, and A. A. Elserougi, "An improved performance direct-drive permanent magnet wind generator using a novel single-layer winding layout," *IEEE Trans. Magn.*, vol. 49, no. 9, pp. 5124–5134, Sep. 2013.

[18] T. Lubin, S. Mezani, and A. Rezzoug, "2-D exact analytical model for surface-mounted permanent-magnet motors with semi-closed slots," *IEEE Trans. Magn.*, vol. 47, no. 2, pp. 479–492, Feb. 2011.

[19] T. Lubin, S. Mezani, and A. Rezzoug, "Analytical computation of the magnetic field distribution in a magnetic gear," *IEEE Trans. Magn.*, vol. 46, no. 7, pp. 2611–2621, Jul. 2010.

[20] K. Deb, A. Pratap, S. Agarwal, and T. Meyarivan, "A fast and elitist multiobjective genetic algorithm: NSGA-II," *IEEE Trans. Evol. Comput.*, vol. 6, no. 2, pp. 182–197, Apr. 2002.

[21] M. Popescu and D. G. Dorrell, "Proximity losses in the windings of high speed brushless permanent magnet AC motors with single tooth windings and parallel paths," *IEEE Trans. Magn.*, vol. 49, no. 7, pp. 3913–3916, Jul. 2013.

Jiri Dusek received the B.Eng. and M.Eng. degrees in electrical engineering from the Brno University of Technology, Brno, Czech Republic, in 2008 and 2010, respectively. He is currently pursuing the Ph.D. degree with a focus on design, control, and analysis of electric machines with high torque/power density and magnet-less machines.

He joined the Power Electronics, Machines and Drives Group, The University of Nottingham, Nottingham, U.K., as a Ph.D. Researcher, in 2011. In 2013, he spent six months as a Visiting Researcher with the Politecnico di Torino, Turin, Italy.

Puvan Arumugam received the B.Eng. (Hons.) degree in electrical and electronic engineering from The University of Nottingham, Nottingham, U.K., in 2009, and the Ph.D. degree in electrical machines and drives in 2013.

He is currently a Researcher in electric aircraft propulsion with the Power Electronics, Machines, and Control Group, The University of Nottingham. His current research interests include electrical machines and drives for more electric transportations, electromechanical devices and systems, and analytical computation of electromagnetic fields.

Christopher Brunson (M'12) received the M.Eng. and Ph.D. degrees from The University of Nottingham, Nottingham, U.K., in 2009 and 2014, respectively.

He has developed several fault detection and diagnosis methods for matrix converters. His current research interests include power converters for aerospace applications, high-power density matrix converters, and fault tolerant power electronics for safety critical applications.

Emmanuel K. Amankwah received the B.Sc. degree in electrical and electronic engineering from the Kwame Nkrumah University of Science and Technology, Kumasi, Ghana, in 2006, and the M.Sc. and Ph.D. degrees in electrical engineering and electrical and electronic engineering from The University of Nottingham, Nottingham, U.K., in 2009 and 2013, respectively.

He was with the Electricity Company of Ghana, Accra, Ghana, as a Design Engineer from 2006 to 2008. Since 2013, he has been a Research Fellow in emerging technologies for HVdc power transmission with the Power Electronic Machines and Control Research Group, Faculty of Engineering, The University of Nottingham. His current research interests include power electronics for grid integration and motor drive control.

Tahar Hamiti was born in Larbaâ Nath Irathen, Algeria, in 1979. He received the Ingénieur d'Etat degree in automatic control systems from the Mouloud Mammeri University of Tizi-Ouzou, Tizi Ouzou, Algeria, and the Ph.D. degree in electrical engineering from the University of Nancy I, Nancy, France.

He was a Research Fellow and subsequently a Lecturer with the Power Electronics, Machines and Control Group, The University of Nottingham, Nottingham, U.K., from 2010 to 2015. In 2015, he joined VEDECOM, a French institute for energy transition to work on novel electrical machines for electric and hybrid vehicles. His current research interests include modeling, optimal design, and control of high-performance electrical machines for transportation applications and power generation.

Chris Gerada (M'05) received the Ph.D. degree in numerical modeling of electrical machines from The University of Nottingham, Nottingham, U.K., in 2005.

He was subsequently a Researcher with The University of Nottingham, where he was involved in high-performance electrical drives and the design and modeling of electromagnetic actuators for aerospace applications. Since 2006, he has been the Project Manager of the GE Aviation Strategic Partnership. In 2008, he was appointed as a Lecturer in electrical machines, an Associate Professor in 2011, and a Professor with The University of Nottingham, in 2013. His current research interests include the design and modeling of high-performance electric drives and machines.

Dr. Gerada serves as an Associate Editor of the IEEE TRANSACTIONS ON INDUSTRY APPLICATIONS and is the Chair of the IEEE Industrial Electronics Society Electrical Machines Committee.

IEEE Proof